https://doi.org/10.5194/bg-2019-482
Preprint. Discussion started: 27 January 2020

Biogeosciences Discussions

Lake mixing regime selects methane-oxidation kinetics of the methanotroph assemblage

Magdalena J. Mayr[1,2]*, Matthias Zimmermann[1,2]*, Jason Dey[1], Bernhard Wehrli[1,2] and Helmut Bürgmann[2]

* These authors contributed equally to this work.

[1]Department of Surface Waters—Research and Management, Eawag, Swiss Federal Institute of Aquatic Science and Technology, Kastanienbaum, Switzerland

[2]Institute of Biogeochemistry and Pollutant Dynamics, Department of Environmental Systems Science, ETH Zurich, Swiss Federal Institute of Technology, Zurich, Switzerland

Correspondence to: Magdalena J. Mayr (magdalena.mayr@eawag.ch)

Abstract. In freshwater lakes, large amounts of methane are produced in anoxic sediments. Methane-oxidizing bacteria effectively convert this potent greenhouse gas into biomass and carbon dioxide. These bacteria are present throughout the water column where methane concentrations can range from nanomolar to millimolar concentrations. In this study, we tested the hypothesis that methanotroph assemblages in seasonally stratified lakes are adapted to the contrasting methane concentrations in the epi- and hypolimnion. We further hypothesized that lake overturn would change the methane oxidation kinetics as more methane becomes available in the epilimnion. Together with the change of methane oxidation kinetics, we investigated changes in the transcription of genes encoding methane monooxygenase, the enzyme responsible for the first step of methane oxidation, with metatranscriptomics. We show that the half-saturation constant (K_m) for methane, obtained from laboratory experiments with the natural microbial community, differed by two orders of magnitude between epi- and hypolimnion during stable stratification. During lake overturn, however, the kinetic constants in the epi- and hypolimnion converged along with a change of the transcriptionally active methanotroph assemblage. Conventional particulate methane monooxygenase appeared to be responsible for methane oxidation under different methane concentrations. Our results suggest that methane availability is important for creating niches for methanotroph assemblages with well-adapted methane-oxidation kinetics. This rapid selection and succession of adapted lacustrine methanotroph assemblages allows high methane removal efficiency of more than 90 % to be maintained even under rapidly changing conditions during lake overturn. Consequently, only a small fraction of methane stored in the anoxic hypolimnion is emitted to the atmosphere.

https://doi.org/10.5194/bg-2019-482
Preprint. Discussion started: 27 January 2020

1 Introduction

Lakes are an important source of greenhouse gases with methane emissions contributing a major fraction to the climate impact of lacustrine systems (DelSontro et al., 2018). The oxidation of the strong greenhouse gas methane in freshwater lakes is mainly achieved by methane-oxidizing bacteria (MOB), which have the unique ability to use methane as their sole carbon and energy source (Hanson and Hanson, 1996). In anoxic habitats of seasonally stratified lakes, large amounts of methane, which is produced as a final product of anaerobic organic matter degradation, can accumulate in the oxygen-depleted hypolimnion (Conrad, 2009; Steinsberger et al., 2017). Under stratified conditions, aerobic and sometimes anaerobic MOB oxidize this methane in the water column, thereby preventing diffusive outgassing (Bastviken et al., 2002; Graf et al., 2018; Mayr et al., 2019a). Lake overturn in autumn leads to mixing of the oxygen-rich surface layer with the methane-rich bottom water (Schubert et al., 2012). The simultaneous availability of oxygen and methane promotes growth of MOB in the expanding epilimnion at the surface (Kankaala et al., 2007; Mayr et al., 2019b; Schubert et al., 2012; Zimmermann et al., 2019). The resulting increase in methane oxidation capacity has been shown to be associated with a shift in the MOB assemblage in the epilimnion, which grows fast enough to prevent most of the methane transported into the epilimnion from escaping to the atmosphere (Mayr et al., 2019b; Zimmermann et al., 2019).

In temperate, seasonally stratified lakes, the diverse MOB assemblage shows a clear vertical structure and succession during autumn overturn (Kojima et al., 2009; Mayr et al., 2019b). This suggests that mechanisms of spatial and temporal niche partitioning maintain diversity within this functional group (Mayr et al., 2019a). The differences in the methane and oxygen availability in the two water bodies above and below the oxycline likely place very different demands on the ecophysiology of the resident MOB assemblages. Although previous studies have shown great diversity and adaptability of methane oxidation kinetics (Baani and Liesack, 2008; Dunfield and Conrad, 2000; Lofton et al., 2014; Tveit et al., 2019), the role of different kinetic traits in rapidly changing lake environments has so far not been studied systematically. Here, we hypothesized that kinetic parameters of methane oxidation vary between epi- and hypolimnion and that kinetic parameters vary seasonally together with the MOB assemblage, which would show that methane availability is a driver of methane oxidation kinetics of the MOB assemblage. Further, the methane affinity of lacustrine MOB especially in the epilimnion has implications for the amount of methane outgassing during both, stable stratification and lake overturn.

The first step of methane oxidation is mediated by the methane monooxygenase. Most MOB possess the copper-dependent particulate form of the methane monooxygenase (pMMO). Known isozymes of pMMO have been shown to exhibit different methane oxidation kinetics, including high affinity variants that are able to oxidize methane even at atmospheric concentrations (Baani and Liesack, 2008; Dam et al., 2012). A subset of MOB encode the soluble MMO (sMMO) that has a lower methane affinity than pMMO and has been hypothesized to be used by MOB under high methane concentration, because MOB biomass is assumed to be higher under such conditions leading to copper limitation and a switch to copper-free sMMO (Semrau et al., 2018). The abundance of the sMMO gene has been found to be low in a Lake Rotsee (Guggenheim et al., 2019), but relative transcription between epi- and hypolimnion has not been investigated so far.

In this study we conducted a combined kinetic and metatranscriptomic analysis to test our hypothesis that MOB assemblages show distinct methane oxidation kinetics in the methane-rich hypolimnion compared to the epilimnion with low methane concentrations. Further, we examined the changes in methane oxidation kinetics over time during lake overturn, as more methane becomes available in the epilimnion. To do so, we used ex-situ incubations of the resident microbial community to measure methane-oxidation rates and methane affinity combined with MOB cell counts. In parallel, we applied metagenomics and metatranscriptomics to characterize the MOB assemblage and genes and transcripts involved in the methane oxidation pathway, aiming to link observed changes in methane oxidation kinetics with changes in the MOB population activity. Knowledge about the variability of kinetic parameters of methane oxidation is important to better understand the ecology and

https://doi.org/10.5194/bg-2019-482
Preprint. Discussion started: 27 January 2020

68 physiology of MOB in the environment. Further, our results will inform trait-based or process-based modelling approaches,
69 because a single set of time and space invariant kinetic parameters may not reflect natural conditions adequately.

70 2 Methods

71 2.1 Study site and physicochemical lake profiling

72 Lake Rotsee is a small eutrophic lake in central Switzerland that is 2.5 km long, 200 m wide and has a maximum depth of 16
73 m. For more details see (Schubert et al., 2012). We profiled and sampled the water column during five campaigns in autumn
74 2017 at the deepest point of Lake Rotsee at 47.072 N and 8.319 E. We measured profiles of temperature, conductivity and
75 pressure (depth) with a CTD (RBRmaestro, RBR, Canada). A micro-optode (NTH-PSt1, PreSens, Germany) attached to the
76 CTD measured profiles of oxygen concentrations.

77 2.2 ^{3}H-CH_4 tracer technique

78 We used the radio ^{3}H-CH_4 tracer technique as described in Bussmann et al., (2015) and Steinle et al., (2015) to measure
79 methane oxidation rates and kinetics of the MOB assemblage above and below the oxycline. We added 200 µL of gaseous ^{3}H-
80 CH_4/N_2 mixture (~80 kBq, American Radiolabeled Chemicals, USA). We measured total and water fraction radioactivity in a
81 liquid scintillation counter (Tri-Carb 1600CA, Packard, USA) by adding 1 mL sample to 5 mL Insta-Gel (PerkinElmer,
82 Germany). From these activities, we calculated the methane oxidation rate (r_{MOx}):

83 $$r_{MOx} = [CH_4] \times \frac{A_{H_2O}}{A_{H_2O} + A_{CH_4}} \times \frac{1}{t}$$

84 where t is time, [CH_4] is the concentration of methane and activities (A) were corrected for fractional turnover in killed controls.

85 2.3 Methane oxidation kinetics of microbial community

86 We assumed that the dependence of the methane oxidation rate (r_{MOx}) of the microbial community on the methane
87 concentration can be described by a Monod kinetics:

88 $$r_{MOx} = V_{max} \frac{[CH_4]}{K_M + [CH_4]}$$

89 where V_{max} is the maximum methane oxidation rate and K_M is the half-saturation constant for methane. We determined the
90 two kinetic parameters in ex-situ incubations of water samples from above and below the oxycline. We collected water from
91 the two depths in 2 L Schott bottles and transported them to the lab dark and cooled. We stripped dissolved methane by
92 bubbling air for 1h. For each depth, we prepared 60 mL incubations with 10 different methane concentrations and a killed
93 control in duplicates. By adding a 500 µL gas bubble from pre-diluted gas stocks we established methane concentrations of
94 0.4 to 60 µM. Gas stocks were prepared by evacuating and flushing 120 mL crimp-sealed serum vials with pure nitrogen gas
95 five times and adding defined volumes of methane gas with gas tight syringes. In the killed controls, we inhibited methane
96 oxidation by adding 1 mL of $ZnCl_2$ (50 % w/v). To start the incubations, we added the ^{3}H-CH_4 tracer as described in the above
97 section. After vigorous shaking for 1 minute, we kept the incubations dark in a shaker with 100 RPM and at the same
98 temperature as measured within the oxycline. After 4 hours, we stopped the incubations by adding 1 mL of $ZnCl_2$ (50 % w/v).
99 We determined the methane oxidation rate in each incubation as described above.

100 We used a non-linear least squares Levenberg-Marquardt algorithm to fit the Monod equation to the data. Outliers in the data
101 were removed using the following criteria: For the replicates of each methane concentration we removed data points (1) with
102 a water fraction radioactivity that was outside 2σ from the average water fraction radioactivity of all replicates, (2) which
103 showed a water fraction radioactivity that was not above 2σ from the background water fraction radioactivity, (3) for which

https://doi.org/10.5194/bg-2019-482
Preprint. Discussion started: 27 January 2020

we had less than two replicates after the removal of outliers, (4) with a resulting methane oxidation rate outside 2σ from the average methane oxidation rate of all replicates, and (5) showing a methane oxidation rate that was higher than the methane oxidation rate measured for the replicates with the highest methane concentration.

The base value of the specific affinity a° is defined as the ratio V_{max}/K_M. We approximated mean and variance of the ratio of the two random variables with known mean and variance using the Taylor expansions given in ref. (Stuart and Ord, 2009).

2.4 In-situ methane oxidation rates of the microbial community

We determined the in-situ methane oxidation rate of the natural microbial community in duplicate ex-situ incubations of water samples from above and below the oxycline. We anaerobically filled water into 60 mL serum vials, and crimp-sealed and transported them to the lab dark and cooled. For each depth, we prepared killed controls with 1 mL of $ZnCl_2$ (50 % w/v) in duplicates in the same way. We started the incubations by adding the ^3H-CH_4 tracer as described above. After vigorous shaking for 1 minute, we kept the incubations dark in a shaker with 100 RPM at the temperature measured within the oxycline. After 4 hours, we stopped the incubations by adding 1 mL of $ZnCl_2$ (50 % w/v).

2.5 Methane concentration measurement

We measured in-situ methane concentrations in the water column using the headspace equilibration method. For each depth, we collected water samples in 120 mL crimp-sealed serum vials with a small amount of $CuCl_2$ to stopp biological activity. We measured methane concentrations in the headspace with a gas chromatograph (Agilent 6890N, USA) equipped with a Carboxen 1010 column (Supelco 10 m × 0.53 mm, USA) and flame ionisation detector. Samples that exceeded the calibration range were diluted with N_2 and measured again. We calculated dissolved methane concentrations according to Wiesenburg and Guinasso, (1979).

2.6 Quantification of methanotroph cells

We investigated the abundance of aerobic methanotrophs by catalysed reporter deposition fluorescence in situ hybridisation after Pernthaler et al., (2002). We fixed water samples of 5 mL with 300 µl sterile filtered (0.2 µm) formaldehyde (2.22% v/v final concentration) for 3 – 6 h on ice. We filtered the samples onto 0.2 µm nuclepore track-etched polycarbonate membrane filters (Whatman, UK), that we dried, and stored at -20 °C until further analysis. We permeabilized cells with lysozyme (10 mg mL^{-1}) at 37 °C for 70 min, and inactivated endogenous peroxidases with 10 mM HCl for 10 min at room temperature. To hybridise the filters, we used a hybridisation buffer (Eller et al., 2001) containing HRP-labelled probes at 46 °C for 2.5 h. Furthermore, the buffer contained either a 1:1:1 mix of Mg84, Mg705, and Mg669 probes targeting methanotrophic *Gammaproteobacteria* or a Ma450 probe targeting methanotrophic *Alphaproteobacteria* (Eller et al., 2001). To amplify the fluorescent signals, we used the green-fluorescent Oregon Green 488 tyramide (OG) fluorochrome (1 µl mL^{-1}) at 37 °C for 30 min. We counterstained hybridised cells with DAPI (20 µl of 1 µg mL^{-1} per filter) for 5 minutes. For microscopy, we used a 4:1 mix of Citifluor AF1 (Electron Microscopy Sciences, Hatfield, PA, USA) and Vectashield (Vector, Burlingame, CA, USA) as mountant. We used an inverted light microscope (Leica DMI6000 B, Germany) at a 1000-fold magnification to quantify MOB cell numbers. For each sample, we took 22 image pairs (DAPI and OG filters) of randomly selected fields of view (FOVs). To detect and count cells we used digital microbial image analysis software Daime 2.0 (Daims, 2009).

2.7 Metagenome and metatranscriptome analysis

We collected lake water with a Niskin bottle and filtered 800 – 2300ml on-site onto 0.2 µm pore size GTTP isopore filters (Merck Millipore Ltd.). These filters were preserved immediately on dry ice and stored at -80 °C until extraction. We extracted DNA and RNA with the Allprep DNA/RNA Mini Kit (Qiagen) and treated RNA with the rigorous option using the Turbo DNA-free kit (Invitrogen) to remove remaining DNA. In January two filters of the hypolimnion sample were extracted and

https://doi.org/10.5194/bg-2019-482
Preprint. Discussion started: 27 January 2020

sequenced separately serving as replicates indicated with Jan (r). RNA yields from the October sampling were deemed insufficient for sequencing as no typical RNA bands were visible during quality control and therefore these samples were omitted from metatransciptome analysis. Metagenomic and metatranscriptomic 150bp paired-end sequencing was done on a NovaSeq 6000 sequencer (Illumina) at Novogene (HK) company limited (Hong Kong, China). Ribosomal RNA was depleted with Ribo-Zero Magnetic Kit (Illumina) prior to sequencing. The co-assembly of metagenomic sequences alone yielded less *pmoA* as well as *pmoB* and *pmoC* sequences than expected, likely due to low coverage. Therefore, we combined predicted genes from both the metagenomic and the metatranscriptomic *de-novo* assembly as described below. Due to low coverage of *pmoA*, *pmoB* and *pmoC* in the metagenome, we used the metagenome only in the assembly process. All further analyses relied on the metatranscriptome.

We removed remaining ribosomal sequences from metatranscriptomic reads with sortmerna v2.1 (Kopylova et al., 2012) and performed quality filtering with trimmomatic v0.35 (Bolger et al., 2014). We co-assembled reads from seven metatranscriptomic libraries using megahit v1.1.3 (Li et al., 2015) with a final k-mer size of 141 and a minimum contig length of 200. This resulted in 2166829 contigs with an average of 672bp and a N50 of 733bp. For quality filtering of metagenomic reads we used prinseq-lite v0.20.4 (Schmieder and Edwards, 2011) with dust filter (30) and a quality mean of 20. Again we performed a co-assembly using megahit of 10 metagenomes (including three October samples without corresponding metatranscriptome) with a final k-mer size of 121 and a minimum contig size of 300bp (4237394 contigs, average 1008bp and N50 of 1250bp). Gene prediction for both co-assemblies was done with prodigal v 2.6.3 (setting: meta, Hyatt et al., 2010). After combining the predicted genes, cd-hit-est v4.6.6 (Li and Godzik, 2006) was used to remove very similar and duplicate (identity 0.99) predicted genes. With Seqkit v0.7.2 (Shen et al., 2016) predicted genes shorter than 400bp were removed. Predicted genes encoding particulate methane monooxygenases were annotated with prokka v1.3 (Seemann, 2014) using the incorporated databases (metagenome option) and diamond blastx v0.9.22 (e-value 10^{-6}, Buchfink et al., 2014) against custom databases for *pmoA*, *pmoB* and *pmoC.* Annotation was manually validated using alignments and the NCBI refseq_protein database (22.4.2019, O'Leary et al., 2016). *pmoA, pmoB and pmoC* variants summing to a cross-sample sum higher than 50 transcripts per million (TPM) were retained. Genes annotated as *pmoA, pmoB and pmoC* variants which were either not the expected gene (manual inspection) or shorter than 300 bp were removed. Genes encoding part of the soluble methane monooxygenase sMMO (*mmoX, mmoY and mmoZ*) were annotated with prokka v1.3 using incorporated databases and the metagenome option. Paired-end metatranscriptomic reads were mapped to the predicted genes using bbmap v35.85 (Bushnell, 2014) at an identity of 0.99 without mapping of ambiguous reads, and then converted with samtools v1.9 (Li et al., 2009) and counted with featurecounts (Liao et al., 2014) of subread v1.6.4 package (-p option). The count table was normalized within samples to transcripts per million (TPM. Wagner et al., 2012) by first dividing the counts by gene length, then the result by gene was divided by the sum of all results times one million. The TPM values were used to produce the figures in R.

3 Results and discussion

3.1 Environmental conditions during the autumn overturn

From October 2017 to January 2018 the epilimnion depth in Lake Rotsee gradually increased from 5.5 to 13.7 m (Fig. 1a-d). This process of vertical mixing continuously transferred methane that was stored below the oxycline into the epilimnion above. The gradual progression of the autumn overturn stimulates the growth of a distinct MOB assemblage in the epilimnion above the oxycline in response to an influx of methane from the hypolimnion as shown in previous work of Lake Rotsee (Mayr et al., 2019b; Zimmermann et al., 2019). Despite this continuous supply, measured methane concentrations above the oxycline remained below 1 µM (Fig. 1a-d, orange arrows). The low methane concentrations are an indication of intense methane oxidation by the growing MOB assemblage in the epilimnion. The oxygen concentration shifted from 15% oversaturation in October to 67% undersaturation in December (Fig. 1a-d). Aerobic methane oxidation likely contributed to this oxygen

https://doi.org/10.5194/bg-2019-482
Preprint. Discussion started: 27 January 2020

184 depletion in the epilimnion. In the hypolimnion oxygen concentrations were found to be below the detection limit (20 nM)
185 (Kirf et al., 2014) from October to December. However, oxygen may be produced in the hypolimnion by phytoplankton (Brand
186 et al., 2016; Oswald et al., 2015).

187 The two water bodies above and below the oxycline have distinct biogeochemical conditions posing very different demands
188 on the ecophysiology of the MOB assemblage. The hypolimnion contained up to a few hundred micromolar of methane but
189 the flux of oxygen into the hypolimnion was limited due to stratification and low light levels for photosynthesis. On the other
190 hand, the epilimnion contained comparably high oxygen concentrations, but methane concentrations remained low as methane
191 was supplied slowly and was rapidly diluted in the large volume of the epilimnion. In addition, the temperature of the
192 epilimnion dropped from 16 °C to 5 °C, whereas the hypolimnion remained cold (5 - 8 °C). Temperature profiles are shown
193 in Supplementary Fig. 1. A previous study investigating 16S rRNA genes and *pmoA* transcripts indeed revealed niche
194 differentiation of the MOB assemblage between the two water bodies above and below the oxycline with a shift in the MOB
195 assemblage during the overturn (Mayr et al., 2019b).

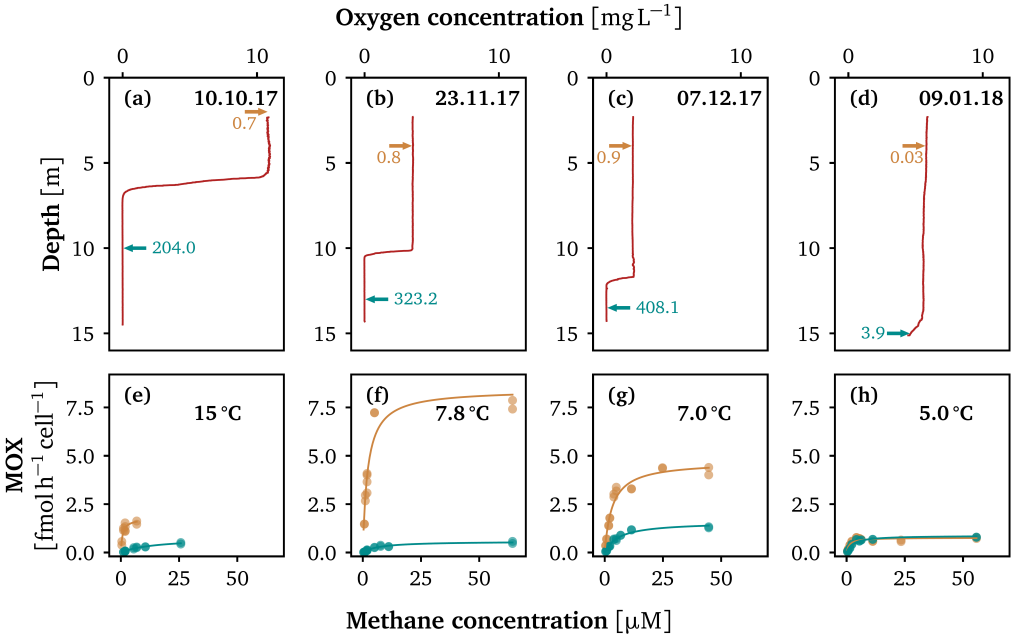

Figure 1. Substrate concentrations and methane oxidation rates during lake overturn in Rotsee. (a - d) Oxygen concentration profiles during the four field campaigns at the dates indicated. The sampling depths above (orange) and below (cyan) the oxycline are indicated by arrows. Numbers next to the arrows represent methane concentrations in µM at the respective depths. (e - h) Cell-specific methane oxidation rates (MOX) of water samples incubated with different methane concentrations. Lines indicate least-square fits of the Monod kinetics. For each campaign, we incubated samples from both depths close to in-situ temperature (indicated in bold).

196 **3.2 Succession of kinetically different microbial communities**

197 Along with the differences in the physical and chemical properties of the two water bodies, we observed a significant difference
198 in the methane oxidation kinetics of the MOB assemblages. From the methane oxidation rates shown in Fig. 1e-h we derived
199 the parameters of Monod kinetics (Fig. 2). These kinetic parameters allowed us to characterize the MOB assemblages above
200 and below the oxycline physiologically and to relate these results to the biogeochemical conditions. The curves describing the
201 methane oxidation kinetics of the MOB assemblages above and below the oxycline did not intersect (except at the origin) in

https://doi.org/10.5194/bg-2019-482
Preprint. Discussion started: 27 January 2020

October and November (Fig. 1e-g). This means that the MOB assemblage in the epilimnion showed both a higher affinity for methane (Fig. 2a) and a higher cell-specific maximum methane oxidation rate (Fig. 2b) than the assemblage below the oxycline. The higher methane affinity is in line with the methane-deficient conditions in the epilimnion. But the fact that both affinity and maximum rate are higher suggests that there were likely additional mechanisms or traits, like adaptation to oxygen concentration or temperature (Hernandez et al., 2015; Trotsenko and Khmelenina, 2005), that prevent the epilimnetic MOB assemblage from invading the assemblage in the hypolimnion. At the end of the overturn period (Fig. 1h) both MOB assemblages showed very similar methane oxidation kinetics.

The pronounced difference in K_m of the two assemblages in October, when the lake was still stratified, gradually converged during lake overturn from November to January (Fig. 2a). From October to January, the half-saturation constant for methane decreased from 15 to 2.7 µM for the hypolimnetic assemblage, but increased from 0.7 to 1.2 µM in the epilimnion, with higher K_m values in November and December (Fig. 2a). A table summarizing the measured methane oxidation kinetics can be found in Supplementary Table 1. The half saturation constants (K_m) in the hypolimnion from October to December (15.2 ± 7.1 µM, 7.1 ± 2.3 µM, 6.1 ± 1.7 µM) were comparable to K_m values of hypolimnion samples (one meter above sediment) in two shallow arctic lakes by Lofton et al., (2014). These authors measured values of 4.45 ± 2.36 µM and 10.61 ± 2.03 µM. Also in the same range, K_m values of 5.5 µM and 44 µM were measured in the last meter above the sediment in a boreal lake (Liikanen et al., 2002) and similar values were found for lake sediments (Kuivila et al., 1988; Remsen et al., 1989). In contrast, the epilimnion K_m in Rotsee in October was 0.7 ± 0.5 µM, which is far lower than K_m values measured in previous studies on lacustrine systems, suggesting a well-adapted MOB assemblage with relatively high affinity in the epilimnion. In soils even higher affinities have been measured (0.056 – 0.186 µM) (Dunfield et al., 1999) and a high-affinity *Methylocystis* strain has been found to have a K_m of 0.11 µM (Baani and Liesack, 2008). Even when the lake overturn was ongoing in November and December, K_m values in the epilimnion stayed in the lower range of previously reported K_m values (2.1 ± 0.9 µM, 3.3 ± 0.9 µM), which underlines the adaptation of the MOB assemblage to the continuously lower methane concentrations in the epilimnion.

In contrast to the substrate affinity, the maximum cell-specific methane oxidation rate started at similar levels in the stratified lake (Fig. 2b). As methane entered the epilimnion in November, the cell-specific V_{max} of the MOB assemblage in this layer was almost 15 times faster than the hypolimnion assemblage, which ensured a fast methane oxidation rate in the epilimnion close to the surface during this critical phase. As a consequence, methane concentrations and emissions remain low (Zimmermann et al., 2019). Towards the end of the lake overturn, when the thermocline had moved to 15 m depth and the two MOB assemblages were most likely homogenized, methane oxidation rates decreased again. By contrast, the cell-specific methane oxidation rate in the hypolimnion remained rather constant throughout the overturn from November to December.

https://doi.org/10.5194/bg-2019-482
Preprint. Discussion started: 27 January 2020

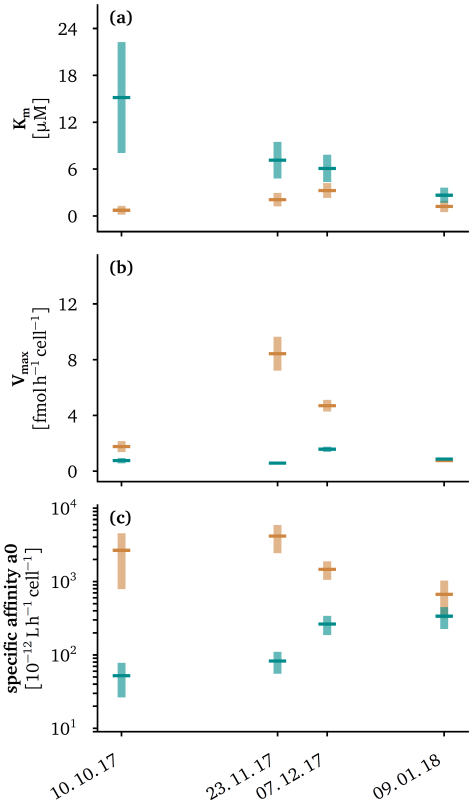

Figure 2. Kinetic properties of the methanotroph assemblage above (orange) and below (cyan) the oxycline for the four sampling campaigns at in-situ temperatures of the oxycline. Lines indicate average values; bars represent the 95% confidence interval. The methane oxidation half-saturation constants (K_m) are displayed in panel (a), maximum cell-specific methane oxidation rates in panel (b) and specific affinities, defined as the ratio V_{max}/K_m, in panel (c).

The specific affinity (V_{max}/K_m) is the initial slope of the hyperbolic Monod kinetics (Button et al., 2004) and is a pseudo first order rate constant for the methane oxidation rate at limiting methane concentrations. The specific affinity towards methane again suggested that the two communities started out very differently and gradually converged to very similar kinetic properties (Fig. 2c). The convergence of the specific affinity was driven by changes of both, K_m and V_{max} of the MOB assemblage in the epilimnion. The final convergence of the specific affinity of both assemblages is in good agreement with the fact that the two water masses become increasingly similar in terms of substrate availability and temperature towards the end of the lake overturn. The emerging kinetic properties might therefore be the result of a converging succession of the two MOB assemblages. The specific affinity measured for various methanotrophic bacteria are typically in the range of 1 to 40 x 10^{-12} L h^{-1} $cell^{-1}$ (Dunfield and Conrad, 2000; Knief and Dunfield, 2005; Tveit et al., 2019) with a few exceptions where specific affinities of up to 600 x 10^{-12} L h^{-1} $cell^{-1}$ were reported (Calhoun and King, 1997). The specific affinities of 52 – 338 x 10^{-12} L h^{-1} $cell^{-1}$, of the MOB assemblage in the hypolimnion were well in the range of these reported values. However, the MOB assemblage in the epilimnion showed much higher specific affinities suggesting that these assemblages were well adapted to the very methane limited conditions in the epilimnion.

Methanotroph cell counts suggest that both the MOB assemblage above and below the oxycline were actively growing over the course of the overturn. In the epilimnion the abundance of MOB increased from 0.1x10^5 to 2x10^5 cells mL^{-1} from October to December, below the oxycline the abundance increased from 0.8x10^5 to 1.2x10^5 cells mL^{-1}. The *in-situ* methane oxidation rates (Supplementary Table 1) of the MOB assemblage in the epilimnion accounted for about 25 % (median) of the maximum methane oxidation rate from October to December. For the MOB assemblage in the hypolimnion, the *in-situ* methane oxidation

https://doi.org/10.5194/bg-2019-482
Preprint. Discussion started: 27 January 2020

Biogeosciences Discussions Open Access EGU

rates were 93 % (median) of the maximum methane oxidation rate. This suggests that the growth of the MOB assemblage in the epilimnion was generally methane limited, despite their higher methane affinity.

3.3 Dynamics of the MOB assemblage and variants of pMMO

Methane oxidation during lake overturn was performed by diverse assemblages of MOB as determined by metatranscriptomic analysis (Fig. 3a1-c1). Thus, the reported kinetics reflect aggregate properties of the respective assemblage. In line with previous lake studies (Biderre-Petit et al., 2011; Mayr et al., 2019a; Sundh et al., 2005), the majority of *pmoCAB* variants were associated with type Ia MOB (*Gammaproteobacteria*). In addition, one variant associated with type Ib MOB (*Gammaproteobacteria*) and up to three variants associated with type II MOB (*Alphaproteobacteria*) were found (Supplementary Table 2), but these only showed a low abundance and decreasing trend. Evidence for the presence or expression of previously described high affinity pMMO (Baani and Liesack, 2008) was not found in the metagenomic or metatranscriptomic dataset. We detected sMMO genes (*mmoXYZ*) but transcription was very low (maximum of 6 TPM per sample, Supplementary Table 3) compared to pMMO. This raises the question under which conditions MOB express sMMO. On the transcript and peptide level the expression of this enzyme is often very low or undetectable under environmental conditions (Cheema et al., 2015; Dumont et al., 2013; Taubert et al., 2019). Our results suggest that conventional pMMO was the main enzyme responsible for methane oxidation under different methane concentrations and environmental conditions in the lake water column.

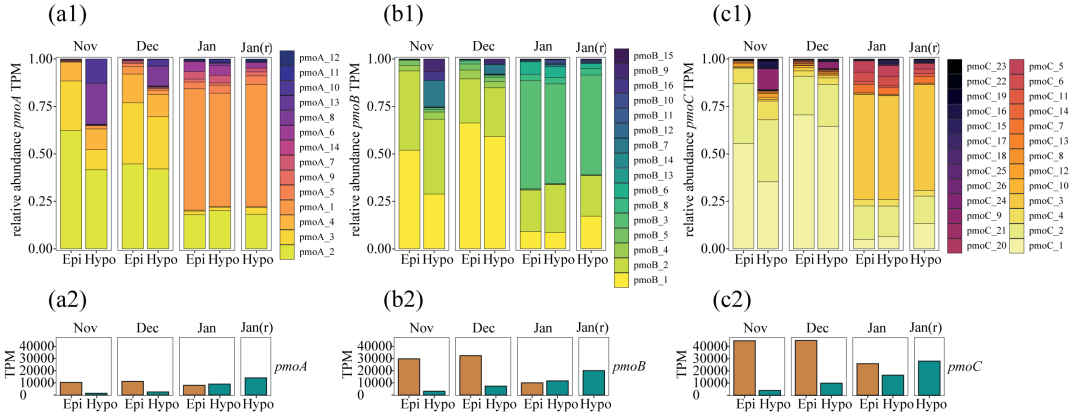

Figure 3. Transcriptional activity of genes encoding pMMO in November, December and January 2017/2018 during overturn in Rotsee. The January hypolimnion sample was measured twice and the replicate is labelled as Jan (r). Relative abundance of gene variants of (a1) *pmoA*, (b1) *pmoB*, (c1) *pmoC* based on transcripts per million (TPM), mapped at 99% identity. *pmoCAB* variants were assembled from metagenomes and metatranscriptomes samples originating from the same depths and dates as shown in Fig. 1. Different color schemes were chosen for *pmoA*, *pmoB* and *pmoC* variants. (a2) *pmoA*, (b2) *pmoB*, (c2) *pmoC* shown as summed TPM of all variants for epi- and hypolimnion (orange and cyan, respectively). Epi = epilimnion, Hypo = hypolimnion.

In November, and to a lesser degree in December, the composition of transcribed *pmoCAB* gene variants differed between epi- and hypolimnion, with some variants (e.g. pmoA_8 and 10, pmoB_7, 9 and 16, pmoC_9, 16, 22) being confined to the hypolimnion (Fig. 3a1-c1). The difference in gene transcription reflects changes in the MOB assemblage (see detrended correspondence analysis in Supplementary Fig. 2), which may explain the observed differences in methane-affinity (Fig. 2). Notably however, a prominent proportion of the *pmoCAB* gene variants transcribed in the epilimnion were also present in high abundance in the hypolimnion, which likely reflects the increasing influence of the highly transcriptionally active epilimnion assemblage (Fig. 3a2-c2) on the hypolimnion assemblage during lake overturn (Mayr et al., 2019b). Unfortunately, we do not have information on the assemblage for the October sampling where the half saturation constants differed most between epi-

https://doi.org/10.5194/bg-2019-482
Preprint. Discussion started: 27 January 2020

and hypolimnion. However, based on observations of the overturn period the year before (Mayr et al., 2019b), it can be assumed that the two layers harboured distinct MOB assemblages also in October, possibly with less overlap.

The composition of transcribed *pmoCAB* variants showed a distinct change over time (Fig. 3a1-c1 and Supplementary Fig. 2). The relative abundance of the *pmoCAB* variants that were specific to the hypolimnion decreased until January (Fig. 3a1-c1) and the two MOB assemblages became increasingly similar in terms of their kinetical properties (Fig. 2). From December to January another strong shift in the MOB assemblage towards dominance of pmoA_1, pmoB_3 and pmoC_3 occurred. This did however not change the methane affinity much (Fig. 2), suggesting that different MOB assemblages can have similar methane affinities. The shift of the MOB assemblage was accompanied by a drop in temperature and rise in oxygen, which are probable drivers of MOB succession in addition to methane availability (Hernandez et al., 2015; Oshkin et al., 2015; Trotsenko and Khmelenina, 2005). With this shift, we also observed a decrease in V_{max} per cell (Fig. 2B). We attribute this to a shift from growth-oriented MOB dominating the bloom phase to a late-successional MOB assemblage adapted to cold temperatures as observed the year before (Mayr et al., 2019b). Further, the metatranscriptomic analysis supports the interpretation that the observed differences in methane oxidation kinetic parameters between water layers and over time have a basis in compositional differences of the transcriptionally active MOB assemblages.

4 Conclusions

In Lake Rotsee, as in many other stratified lakes, the high methane availability in the hypolimnion contrasts with low methane availability in the epilimnion. Therefore, we hypothesized that the resident MOB assemblages are adapted to the respective conditions. Our field study revealed a high level of adaptation of the MOB assemblage: the K_m differed by two orders of magnitude between epi- and hypolimnion during stable stratification. Transcribed methane oxidation genes differed as well, indicating that methane affinity is an important trait structuring MOB assemblages in this system. The MOB assemblage and its kinetic traits adapted rapidly to changing conditions in the epilimnion. In October, the low epilimnion K_m suggested an adaptation to oligotrophic conditions with low methane concentrations. During the autumn overturn, affinity decreased slightly but remained below hypolimnion values, reflecting persistently low methane concentrations that suggest methane-limited growth despite higher methane input. We observed increased V_{max} in the epilimnion during November and December. In this period, continuous transport of methane into the epilimnion provided an advantage of fast-growing MOB over slower competitors. By contrast, in the hypolimnion methane concentrations during overturn exceeded the K_m several-fold suggesting that MOB growth was not limited by methane concentrations.

Our transcriptomic analysis revealed that the variations in methane affinity were entirely linked to *pmoCAB* variants and pMMO appeared to be the dominant methane monooxygenase throughout. We found no evidence for shifts between sMMO and pMMO transcription as hypothesized previously (Semrau et al., 2018) nor could we observe previously described high-affinity pMMO variants, which suggests considerable, so far unappreciated variability in pMMO kinetics. Further research will be needed to obtain kinetic data on individual pMMO variants. However, the provided kinetic parameters for lake MOB assemblages will inform future trait or process-based models of the MOB assemblage and methane emissions. In summary, our work demonstrates that differential methane availability governed by lake mixing regimes creates niches for MOB assemblages with well-adapted methane-oxidation kinetics.

https://doi.org/10.5194/bg-2019-482
Preprint. Discussion started: 27 January 2020

Biogeosciences Discussions Open Access EGU

Figure captions

Figure 1. Substrate concentrations and methane oxidation rates during lake overturn in Rotsee. (a - d) Oxygen concentration profiles during the four field campaigns at the dates indicated. The sampling depths above (orange) and below (cyan) the oxycline are indicated by arrows. Numbers next to the arrows represent methane concentrations in µM at the respective depths. (e - h) Cell-specific methane oxidation rates (MOX) of water samples incubated with different methane concentrations. Lines indicate least-square fits of the Monod kinetics. For each campaign, we incubated samples from both depths close to in-situ temperature (indicated in bold).

Figure 2. Kinetic properties of the methanotroph assemblage above (orange) and below (cyan) the oxycline for the four sampling campaigns at in-situ temperatures of the oxycline. Lines indicate average values; bars represent the 95% confidence interval. The methane oxidation half-saturation constants (K_m) are displayed in panel (a), maximum cell-specific methane oxidation rates in panel (b) and specific affinities, defined as the ratio V_{max}/K_m, in panel (c).

Figure 3. Transcriptional activity of genes encoding pMMO in November, December and January 2017/2018 during overturn in Rotsee. The January hypolimnion sample was measured twice and the replicate is labelled as Jan (r). Relative abundance of gene variants of (a1) *pmoA*, (b1) *pmoB*, (c1) *pmoC* based on transcripts per million (TPM), mapped at 99% identity. *pmoCAB* variants were assembled from metagenomes and metatranscriptomes samples originating from the same depths and dates as shown in Fig. 1. Different color schemes were chosen for *pmoA*, *pmoB* and *pmoC* variants. (a2) *pmoA*, (b2) *pmoB*, (c2) *pmoC* shown as summed TPM of all variants for epi- and hypolimnion (orange and cyan, respectively). Epi = epilimnion, Hypo = hypolimnion.

Data availability

Raw reads of the sequencing project were submitted to the European Nucleotide Archive under project number PRJEB35558. Methane concentrations, scintillation counts, methane oxidation rates, estimated kinetic parameters and the identified nucleotide sequences encoding MMO are available at the EAWAG repository under https://doi.org/10.25678/0001fa (Mayr et al., 2019c).

Author contribution

MJM and MZ contributed equally to this work. MJM, MZ, and HB conceptualized the study and MJM, MZ and JD carried out the investigation. MJM and MZ curated, analyzed and visualized the data. MJM and MZ wrote the original draft of the manuscript with contributions from BW, HB and JD. Funding was acquired by HB.

Competing interests

The authors declare that they have no conflict of interest.

Acknowledgements

This research was funded by the Swiss National Science Foundation (grant CR23I3_156759), by ETH Zurich and Eawag. We are grateful to Andreas Brand for his support and advice in the early stages of the project, to Carsten Schubert, Serge Robert and Daniel Steiner for the possibility and the support to use the equipment for radioisotope and methane measurement. We are also grateful to Lea Steinle for sharing her expertise on how to handle the radiolabeled methane. We would like to thank Karin Beck and Patrick Kathriner for technical assistance during field work and laboratory analysis. We thank Feng Ju and Robert Niederdorfer for advice on the bioinformatics analysis. Sequencing data were analyzed in collaboration with the Genetic Diversity Centre (GDC) of ETH Zurich.

https://doi.org/10.5194/bg-2019-482
Preprint. Discussion started: 27 January 2020

References

Baani, M. and Liesack, W.: Two isozymes of particulate methane monooxygenase with different methane oxidation kinetics are found in Methylocystis sp. strain SC2., Proc. Natl. Acad. Sci. U. S. A., 105(29), 10203–8, doi:10.1073/pnas.0702643105, 2008.

Bastviken, D., Ejlertsson, J. and Tranvik, L.: Measurement of methane oxidation in lakes: A comparison of methods, Environ. Sci. Technol., 36(15), 3354–3361, doi:10.1021/es010311p, 2002.

Biderre-Petit, C., Jézéquel, D., Dugat-Bony, E., Lopes, F., Kuever, J., Borrel, G., Viollier, E., Fonty, G. and Peyret, P.: Identification of microbial communities involved in the methane cycle of a freshwater meromictic lake, FEMS Microbiol. Ecol., 77(3), 533–545, doi:10.1111/j.1574-6941.2011.01134.x, 2011.

Bolger, A. M., Lohse, M. and Usadel, B.: Trimmomatic: A flexible trimmer for Illumina sequence data, Bioinformatics, 30(15), 2114–2120, doi:10.1093/bioinformatics/btu170, 2014.

Brand, A., Bruderer, H., Oswald, K., Guggenheim, C., Schubert, C. J. and Wehrli, B.: Oxygenic primary production below the oxycline and its importance for redox dynamics, Aquat. Sci., 78(4), 727–741, doi:10.1007/s00027-016-0465-4, 2016.

Buchfink, B., Xie, C. and Huson, D. H.: Fast and sensitive protein alignment using DIAMOND, Nat. Methods, 12(1), 59–60, doi:10.1038/nmeth.3176, 2014.

Bushnell, B.: BBMap: a fast, accurate, splice-aware aligner., 2014.

Bussmann, I., Matousu, A., Osudar, R. and Mau, S.: Assessment of the radio ^{3}H-CH_4 tracer technique to measure aerobic methane oxidation in the water column, Limnol. Oceanogr. Methods, 13(6), 312–327, doi:10.1002/lom3.10027, 2015.

Button, D. K., Robertson, B., Gustafson, E. and Zhao, X.: Experimental and Theoretical Bases of Specific Affinity, a Cytoarchitecture-Based Formulation of Nutrient Collection Proposed To Supercede the Michaelis-Menten Paradigm of Microbial Kinetics, Appl. Environ. Microbiol., 70(9), 5511–5521, doi:10.1128/AEM.70.9.5511-5521.2004, 2004.

Calhoun, A. and King, G. M.: Regulation of root-associated methanotrophy by oxygen availability in the rhizosphere of two aquatic macrophytes, Appl. Environ. Microbiol., 63(8), 3051–3058, doi:10.1029/2012WR012444, 1997.

Cheema, S., Zeyer, J. and Henneberger, R.: Methanotrophic and methanogenic communities in swiss alpine fens dominated by Carex rostrata and Eriophorum angustifolium, Appl. Environ. Microbiol., 81(17), 5832–5844, doi:10.1128/AEM.01519-15, 2015.

Conrad, R.: The global methane cycle: Recent advances in understanding the microbial processes involved, Environ. Microbiol. Rep., 1(5), 285–292, doi:10.1111/j.1758-2229.2009.00038.x, 2009.

Daims, H.: Use of fluorescence in situ hybridization and the daime image analysis program for the cultivation-independent quantification of microorganisms in environmental and medical samples, Cold Spring Harb. Protoc., 2009(7), db.prot5253, 2009.

Dam, B., Dam, S., Kube, M., Reinhardt, R. and Liesack, W.: Complete genome sequence of Methylocystis sp. strain SC2, an aerobic methanotroph with high-affinity methane oxidation potential, J. Bacteriol., 194(21), 6008–6009, doi:10.1128/JB.01446-12, 2012.

DelSontro, T., Beaulieu, J. J. and Downing, J. A.: Greenhouse gas emissions from lakes and impoundments: Upscaling in the face of global change, Limnol. Oceanogr. Lett., 3(3), 64–75, doi:10.1002/lol2.10073, 2018.

Dumont, M. G., Pommerenke, B. and Casper, P.: Using stable isotope probing to obtain a targeted metatranscriptome of aerobic methanotrophs in lake sediment, Environ. Microbiol. Rep., 5(5), 757–764, doi:10.1111/1758-2229.12078, 2013.

https://doi.org/10.5194/bg-2019-482
Preprint. Discussion started: 27 January 2020

382 Dunfield, P. F. and Conrad, R.: Starvation alters the apparent half-saturation constant for methane in the type II methanotroph
383 Methylocystis strain LR1, Appl. Environ. Microbiol., 66(9), 4136–4138, doi:10.1128/AEM.66.9.4136-4138.2000, 2000.

384 Dunfield, P. F., Liesack, W., Henckel, T., Knowles, R. and Conrad, R.: High-affinity methane oxidation by a soil enrichment
385 culture containing a type II methanotroph, Appl. Environ. Microbiol., 65(3), 1009–1014, doi:10.3109/17435390.2011.562327,
386 1999.

387 Eller, G., Stubner, S. and Frenzel, P.: Group-specific 16S rRNA targeted probes for the detection of type I and type II
388 methanotrophs by fluorescence in situ hybridisation, FEMS Microbiol. Lett., 198(2), 91–97, doi:10.1016/S0378-
389 1097(01)00130-6, 2001.

390 Graf, J. S., Mayr, M. J., Marchant, H. K., Tienken, D., Hach, P. F., Brand, A., Schubert, C. J., Kuypers, M. M. M. and Milucka,
391 J.: Bloom of a denitrifying methanotroph, 'Candidatus Methylomirabilis limnetica', in a deep stratified lake, Environ.
392 Microbiol., 20(7), 2598–2614, doi:10.1111/1462-2920.14285, 2018.

393 Guggenheim, C., Brand, A., Bürgmann, H., Sigg, L. and Wehrli, B.: Aerobic methane oxidation under copper scarcity in a
394 stratified lake, Sci. Rep., 9(1), 1–11, doi:10.1038/s41598-019-40642-2, 2019.

395 Hanson, R. S. and Hanson, T. E.: Methanotrophic bacteria, Microbiol. Rev., 60(2), 439–471, doi:10.1002/0471263397.env316,
396 1996.

397 Hernandez, M. E., Beck, D. A. C., Lidstrom, M. E. and Chistoserdova, L.: Oxygen availability is a major factor in determining
398 the composition of microbial communities involved in methane oxidation., PeerJ, 3(e801), 1–13, doi:10.7717/peerj.801, 2015.

399 Hyatt, D., Chen, G.-L., LoCascio, P. F., Land, M. L., Larimer, F. W. and Hauser, L. J.: Prodigal: prokaryotic gene recognition
400 and translation initiation site identification, BMC Bioinformatics, 11(119), 1–11, doi:10.3389/fgene.2015.00348, 2010.

401 Kankaala, P., Taipale, S., Nykänen, H. and Jones, R. I.: Oxidation, efflux, and isotopic fractionation of methane during
402 autumnal turnover in a polyhumic, boreal lake, J. Geophys. Res. Biogeosciences, 112(2), 1–7, doi:10.1029/2006JG000336,
403 2007.

404 Kirf, M. K., Dinkel, C., Schubert, C. J. and Wehrli, B.: Submicromolar oxygen profiles at the oxic-anoxic boundary of
405 temperate lakes, Aquat. Geochemistry, 20(1), 39–57, doi:10.1007/s10498-013-9206-7, 2014.

406 Knief, C. and Dunfield, P. F.: Response and adaptation of different methanotrophic bacteria to low methane mixing ratios,
407 Environ. Microbiol., 7(9), 1307–1317, doi:10.1111/j.1462-2920.2005.00814.x, 2005.

408 Kojima, H., Iwata, T. and Fukui, M.: DNA-based analysis of planktonic methanotrophs in a stratified lake, Freshw. Biol.,
409 54(7), 1501–1509, doi:10.1111/j.1365-2427.2009.02199.x, 2009.

410 Kopylova, E., Noé, L. and Touzet, H.: SortMeRNA: Fast and accurate filtering of ribosomal RNAs in metatranscriptomic data,
411 Bioinformatics, 28(24), 3211–3217, doi:10.1093/bioinformatics/bts611, 2012.

412 Kuivila, K. M., Murray, J. W., Devol, A. H., Lidstrom, M. E. and Reimers, C. E.: Methane cycling in the sediments of Lake
413 Washington, Limnol. Oceanogr., 33(4), 571–581, doi:10.4319/lo.1988.33.4.0571, 1988.

414 Li, D., Liu, C. M., Luo, R., Sadakane, K. and Lam, T. W.: MEGAHIT: An ultra-fast single-node solution for large and complex
415 metagenomics assembly via succinct de Bruijn graph, Bioinformatics, 31(10), 1674–1676, doi:10.1093/bioinformatics/btv033,
416 2015.

417 Li, H., Handsaker, B., Wysoker, A., Fennell, T., Ruan, J., Homer, N., Marth, G., Abecasis, G. and Durbin, R.: The Sequence
418 Alignment/Map format and SAMtools, Bioinformatics, 25(16), 2078–2079, doi:10.1093/bioinformatics/btp352, 2009.

419 Li, W. and Godzik, A.: Cd-hit: A fast program for clustering and comparing large sets of protein or nucleotide sequences,

Bioinformatics, 22(13), 1658–1659, doi:10.1093/bioinformatics/btl158, 2006.

Liao, Y., Smyth, G. K. and Shi, W.: FeatureCounts: An efficient general purpose program for assigning sequence reads to genomic features, Bioinformatics, 30(7), 923–930, doi:10.1093/bioinformatics/btt656, 2014.

Liikanen, A., Huttunen, J. T., Valli, K. and Martikainen, P. J.: Methane cycling in the sediment and water column of mid-boreal hyper-eutrophic Lake Kevätön, Finland, Fundam. Appl. Limnol., 154(4), 585–603, doi:10.1127/archiv-hydrobiol/154/2002/585, 2002.

Lofton, D. D., Whalen, S. C. and Hershey, A. E.: Effect of temperature on methane dynamics and evaluation of methane oxidation kinetics in shallow Arctic Alaskan lakes, Hydrobiologia, 721(1), 209–222, doi:10.1007/s10750-013-1663-x, 2014.

Mayr, M. J., Zimmermann, M., Guggenheim, C., Brand, A. and Bürgmann, H.: Niche partitioning of methane-oxidizing bacteria along the oxygen–methane counter gradient of stratified lakes, ISME J., doi:10.1038/s41396-019-0515-8, 2019a.

Mayr, M. J., Zimmermann, M., Dey, J., Brand, A. and Bürgmann, H.: Growth and rapid succession of methanotrophs effectively limit methane release during lake overturn, bioRxiv, doi:https://doi.org/10.1101/707836, 2019b.

Mayr, M. J., Zimmermann, M., Dey, J., Wehrli, B. and Bürgmann, H.: Data for: Community methane-oxidation kinetics selected by lake mixing regime [Data set], Eawag Swiss Fed. Inst. Aquat. Sci. Technol., doi:10.25678/0001fa, 2019c.

O'Leary, N. A., Wright, M. W., Brister, J. R., Ciufo, S., Haddad, D., McVeigh, R., Rajput, B., Robbertse, B., Smith-White, B., Ako-Adjei, D., Astashyn, A., Badretdin, A., Bao, Y., Blinkova, O., Brover, V., Chetvernin, V., Choi, J., Cox, E., Ermolaeva, O., Farrell, C. M., Goldfarb, T., Gupta, T., Haft, D., Hatcher, E., Hlavina, W., Joardar, V. S., Kodali, V. K., Li, W., Maglott, D., Masterson, P., McGarvey, K. M., Murphy, M. R., O'Neill, K., Pujar, S., Rangwala, S. H., Rausch, D., Riddick, L. D., Schoch, C., Shkeda, A., Storz, S. S., Sun, H., Thibaud-Nissen, F., Tolstoy, I., Tully, R. E., Vatsan, A. R., Wallin, C., Webb, D., Wu, W., Landrum, M. J., Kimchi, A., Tatusova, T., DiCuccio, M., Kitts, P., Murphy, T. D. and Pruitt, K. D.: Reference sequence (RefSeq) database at NCBI: Current status, taxonomic expansion, and functional annotation, Nucleic Acids Res., 44(D1), D733–D745, doi:10.1093/nar/gkv1189, 2016.

Oshkin, I. Y., Beck, D. A. C., Lamb, A. E., Tchesnokova, V., Benuska, G., Mctaggart, T. L., Kalyuzhnaya, M. G., Dedysh, S. N., Lidstrom, M. E. and Chistoserdova, L.: Methane-fed microbial microcosms show differential community dynamics and pinpoint taxa involved in communal response, ISME J., 9(5), 1119–1129, doi:10.1038/ismej.2014.203, 2015.

Oswald, K., Milucka, J., Brand, A., Littmann, S., Wehrli, B., Kuypers, M. M. M. and Schubert, C. J.: Light-dependent aerobic methane oxidation reduces methane emissions from seasonally stratified lakes, PLoS One, 10(7), 1–22, doi:10.1371/journal.pone.0132574, 2015.

Pernthaler, A., Pernthaler, J. and Amann, R.: Fluorescence In Situ Hybridization and Catalyzed Reporter Deposition for the Identification of Marine Bacteria, Appl. Environ. Microbiol., 68(6), 3094–3101, doi:10.1128/AEM.68.6.3094, 2002.

Remsen, C. C., Minnich, E. C., Stephens, R. S., Buchholz, L. and Lidstrom, M. E.: Methane Oxidation in Lake Superior Sediments, J. Great Lakes Res., 15(1), 141–146, doi:10.1016/S0380-1330(89)71468-4, 1989.

Schmieder, R. and Edwards, R.: Quality control and preprocessing of metagenomic datasets, Bioinformatics, 27(6), 863–864, doi:10.1093/bioinformatics/btr026, 2011.

Schubert, C. J., Diem, T. and Eugster, W.: Methane emissions from a small wind shielded lake determined by eddy covariance, flux chambers, anchored funnels, and boundary model calculations: A comparison, Environ. Sci. Technol., 46(8), 4515–4522, doi:10.1021/es203465x, 2012.

Seemann, T.: Prokka: Rapid prokaryotic genome annotation, Bioinformatics, 30(14), 2068–2069,

458 doi:10.1093/bioinformatics/btu153, 2014.

459 Semrau, J. D., DiSpirito, A. A., Gu, W. and Yoon, S.: Metals and methanotrophy, Appl. Environ. Microbiol., 84(6), 7–14,
460 doi:10.1128/AEM.02289-17, 2018.

461 Shen, W., Le, S., Li, Y. and Hu, F.: SeqKit: A cross-platform and ultrafast toolkit for FASTA/Q file manipulation, PLoS One,
462 11(10), 1–10, doi:10.1371/journal.pone.0163962, 2016.

463 Steinle, L., Graves, C. A., Treude, T., Ferré, B., Biastoch, A., Bussmann, I., Berndt, C., Krastel, S., James, R. H., Behrens, E.,
464 Böning, C. W., Greinert, J., Sapart, C. J., Scheinert, M., Sommer, S., Lehmann, M. F. and Niemann, H.: Water column
465 methanotrophy controlled by a rapid oceanographic switch, Nat. Geosci., 8(5), 378–382, doi:10.1038/ngeo2420, 2015.

466 Steinsberger, T., Schmid, M., Wüest, A., Schwefel, R., Wehrli, B. and Müller, B.: Organic carbon mass accumulation rate
467 regulates the flux of reduced substances from the sediments of deep lakes, Biogeosciences, 14(13), 3275–3285,
468 doi:10.5194/bg-14-3275-2017, 2017.

469 Stuart, A. and Ord, J. K.: Kendall's Advanced Theory of Statistics: Volume 1: Distribution Theory, Wiley., 2009.

470 Sundh, I., Bastviken, D. and Tranvik, L. J.: Abundance, activity, and community structure of pelagic methane-oxidizing
471 bacteria in temperate lakes, Appl. Environ. Microbiol., 71(11), 6746–6752, doi:10.1128/AEM.71.11.6746-6752.2005, 2005.

472 Taubert, M., Grob, C., Crombie, A., Howat, A. M., Burns, O. J., Weber, M., Lott, C., Kaster, A., Vollmers, J., Jehmlich, N.,
473 von Bergen, M., Chen, Y. and Murrell, J. C.: Communal metabolism by Methylococcaceae and Methylophilaceae is driving
474 rapid aerobic methane oxidation in sediments of a shallow seep near Elba, Italy , Environ. Microbiol., 00, doi:10.1111/1462-
475 2920.14728, 2019.

476 Trotsenko, Y. A. and Khmelenina, V. N.: Aerobic methanotrophic bacteria of cold ecosystems, FEMS Microbiol. Ecol., 53(1),
477 15–26, doi:10.1016/j.femsec.2005.02.010, 2005.

478 Tveit, A. T., Hestnes, A. G., Robinson, S. L., Schintlmeister, A., Dedysh, S. N., Jehmlich, N., Von Bergen, M., Herbold, C.,
479 Wagner, M., Richter, A. and Svenning, M. M.: Widespread soil bacterium that oxidizes atmospheric methane, Proc. Natl.
480 Acad. Sci. U. S. A., 116(17), 8515–8524, doi:10.1073/pnas.1817812116, 2019.

481 Wagner, G. P., Kin, K. and Lynch, V. J.: Measurement of mRNA abundance using RNA-seq data: RPKM measure is
482 inconsistent among samples, Theory Biosci., 131(4), 281–285, doi:10.1007/s12064-012-0162-3, 2012.

483 Wiesenburg, D. A. and Guinasso, N. L.: Equilibrium solubilities of methane, carbon monoxide, and hydrogen in water and sea
484 water, J. Chem. Eng. Data, 24(4), 356–360, doi:10.1021/je60083a006, 1979.

485 Zimmermann, M., Mayr, M. J., Bouffard, D., Eugster, W., Steinsberger, T., Wehrli, B., Brand, A. and Bürgmann, H.: Lake
486 overturn as a key driver for methane oxidation, bioRxiv, 689182, doi:10.1101/689182, 2019.

487